Journal of Advanced Research 25 (2020) 49–56

Contents lists available at ScienceDirect

Journal of Advanced Research

journal homepage: www.elsevier.com/locate/jare

Fractional-order modeling of lithium-ion batteries using additive noise assisted modeling and correlative information criterion ☆

Meijuan Yu [a], Yan Li [a,*], Igor Podlubny [b], Fengjun Gong [a], Yue Sun [a], Qi Zhang [a], Yunlong Shang [a], Bin Duan [a], Chenghui Zhang [a]

[a] School of Control Science and Engineering, Shandong University, Jinan 250061, China
[b] BERG Faculty, Technical University of Kosice, B. Nemcovej 3, 04200 Kosice, Slovakia

HIGHLIGHTS

- Present an integrative modeling method regarding structure, parameters and states.
- Parameterization by using online/offline EIS and iterative learning optimization.
- Introduce 1/*f* noise to reveal correlations among parameters and eigen-voltages.
- Provide the correlative information criterion to evaluate various battery models.
- Present the strong negative correlation of ohmic resistance and state of health.

GRAPHICAL ABSTRACT

The fractional-order modeling with structure identification, parameter estimation and the ability of revealing natures of battery are considered. The correlative information criterion is proposed based on the 1/*f* noise assisted I/O data, which is adept in evaluating the reliability of model structure and adaptiveness of model parameters. Experimental results validate the above conclusions.

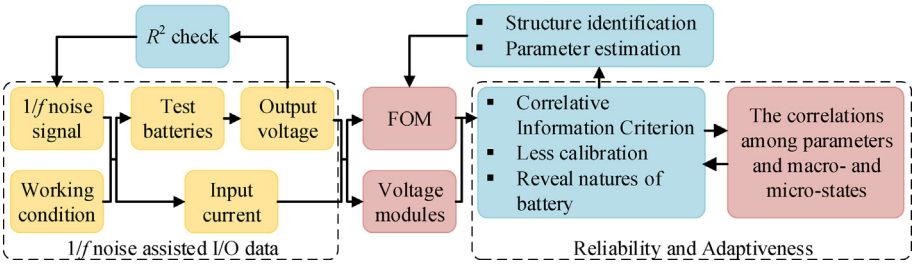

ARTICLE INFO

Article history:
Received 11 March 2020
Revised 6 June 2020
Accepted 7 June 2020
Available online 20 June 2020

Keywords:
Fractional-order modeling
Electrochemical impedance spectroscopy
Iterative learning identification
Weighted co-expression network analysis
Correlative information criterion

ABSTRACT

In this paper, the fractional-order modeling of multiple groups of lithium-ion batteries with different states is discussed referring to electrochemical impedance spectroscopy (EIS) analysis and iterative learning identification method. The structure and parameters of the presented fractional-order equivalent circuit model (FO-ECM) are determined by EIS from electrochemical test. Based on the working condition test, a P-type iterative learning algorithm is applied to optimize certain selected model parameters in FO-ECM affected by polarization effect. What's more, considering the reliability of structure and adaptiveness of parameters in FO-ECM, a pre-tested nondestructive 1/*f* noise is superimposed to the input current, and the correlative information criterion (CIC) is proposed by means of multiple correlations of each parameter and confidence eigen-voltages from weighted co-expression network analysis method. The tested batteries with different state of health (SOH) can be successfully simulated by FO-ECM with rarely need of calibration when excluding polarization effect. Particularly, the small value of CIC_{α} indicates that the fractional-order α is constant over time for the purpose of SOH estimation. Meanwhile, the time-varying ohmic resistance R_0 in FO-ECM can be regarded as a wind vane of SOH due to the large value of CIC_{R_0}. The above analytically found parameter-state relations are highly consistent with the

☆ This work is supported by the Innovative Research Groups of National Natural Science Foundation of China (61821004), National Natural Science Foundation of China (U1964207, 61973193, 61527809, U1764258, U1864205), and Young Scholars Program of Shandong University. Igor Podlubny is supported by grants APVV-18-0526, APVV-14-0892, VEGA 1/0365/19, and COST CA15225.

* Corresponding author.
E-mail address: liyan_cse@sdu.edu.cn (Y. Li).

https://doi.org/10.1016/j.jare.2020.06.003

existing literature and empirical conclusions, which indicates the broad application prospects of this paper.

Introduction

With the huge consumption of fossil energy and increasing environmental pollution problems, many policies and measures have been put forward to promote the development of clean energy industries [1], particularly that the widely promoted electric vehicles have attracted significant attentions [2,3]. The battery as the main power source of electric vehicles plays a crucial role in the safety, performance and economy of electric vehicles. Among various power batteries, lithium-ion battery is still leading the mainstream due to its high energy density, high power density, low self-discharge rate, long cycle life, etc [4]. Moreover, the safe, reliable and stable operation of battery depends on the battery management system (BMS) that is embedded to monitor the operating environments and to diagnose the states of batteries, such as State of Charge (SOC), State of Health (SOH), etc [5]. These states cannot be directly measured, but closely depend on model-based estimation algorithms [6–8].

The commonly used battery models mainly fall into three categories: electrochemical models [9–11], data-driven models [12,13] and equivalent circuit models (ECMs) [14–16]. Electrochemical models always have high accuracy and can describe the complex electrochemical reaction mechanism in battery using a number of partial differential equations (PDEs). But they are unsuitable for electrical design and simulation, because these dimensionless PDEs as well as some specific first principles are inconvenient to represent the electrical performance parameters, or requires large loads of memory and computation [17]. Moreover, the data-driven models describe the battery as a black box, and pay attentions to the mapping relation of the external input and output characteristics. However, the model error is susceptible by training data or methods, and a large number of experimental data are required for model training. Furthermore, according to the physical characteristics of the battery, ECMs can simulate the $I-V$ characteristics of the battery by using a number of equivalent circuits composing of resistance, capacitance, voltage source and so on [18,19]. These models have been widely used in BMS and battery test system taking the advantages of fewer parameters, higher accuracy and easy to calculate [20].

It is well known that the accuracy of ECMs can be improved by adding certain number of resistance–capacitance (RC) pairs [20]. Nevertheless, the blindly adding of RC pairs not only improves the risk of over fitting, but also blurs out the physical meanings of parameters. Thus, it is utmost important to select the structure of model with the balance of the accuracy and complexity [21,22]. The Akaike information criterion (AIC) and Bayes information criterion (BIC) as well as their extensions [23,24] have been widely used to identify the optimal model structure for linear and nonlinear models [17,20]. In addition, with the introduce of fractional-order element [25], the fractional-order models have received huge amount of attentions thanks to their high fitting accuracy of complex dynamic processes. [19] proposes a fractional-order model (FOM) for lithium-ion battery with high accuracy and robustness. [26] presents the principles of fractional-order modeling for dynamic processes by using electrochemical impedance spectroscopy (EIS). EIS also has been applied for analyzing and modeling fractional-order systems, such as analyzing complex physical and chemical processes occurring within electrochemical systems [27] as well as characterization of materials [28,29]. An EIS inspired empirical FOM for lithium-ion batteries is proposed in [30]. Moreover, compared with various external characteristic fitting methods [31,32], [33] proposes the parameter identification method for the fractional-order first-order RC model referring to the relations between complex electrochemical actions within battery and the electrical elements in FOM. And the dependency of model parameters on battery states and external conditions is presented by EIS [34]. Therefore, FOM is an efficient and practical tool for the battery modelings, whose cores are the structure identification, parameter estimation and ability of revealing natures of battery.

The overall structure of this paper is shown in Fig. 1. For the sake of three core reasons at FOMs, the CIC algorithm is proposed and used to indicate the reliability of model structure as well as reveal the correlations among model parameters and battery states. Meanwhile, the nondestructive $1/f$ noise assisted input current and output voltage are obtained through testing batteries, and the $1/f$ noise signal needs to be optimized by R^2 check. The three main contributions of this paper are summarized as.

(1) **Fractional-order modeling:** The EIS is analyzed for structure identification and parameter estimation of FOM. ILI is applied to optimize fractional-order α and polarization response parameters.
(2) **Nondestructive noise and CIC:** The nondestructive $1/f$ noise is optimized subject to the R^2 index. The noise assistant output voltages lead to eigen-voltages by using WCNA. The multiple correlation coefficients between eigen-voltages and model parameters are defined as CIC indices.
(3) **CIC based model evaluation:** The CIC indices of parameters indicate the reliability of model structure and adaptiveness of parameters. These indices can also reveal qualitative relations between model parameters and battery states.

The remainder of this paper is organized as follows. In Section "Battery test platform", the battery test and data acquisition platforms are described. In Section "Fractional-order Modeling", the structure identification and parameter estimation of FOM are discussed. The correlation analysis and correlative information criterion are presented in Section "Model evaluat", and the conclusions are given in Section "Conclusions".

Battery test platform

Battery test bench

As shown in Fig. 2, the battery test bench consists of an electrochemical workstation (Autolab), a battery test platform (AVL or Arbin), a thermal chamber and a computer. The electrochemical workstation is used to acquire EIS. The battery test platform implements battery characteristic test that provides data of input current, output voltage and states of batteries. The thermal chamber is applied to ambient temperature control. The computer is for experimental control (programmable input signal, etc) and data acquisition through CAN bus.

In this paper, all of the battery tests are carried out with constant temperature 25 °C. In the electrochemical test for EIS, the battery is in a static state, and the impedance characteristic of bat-

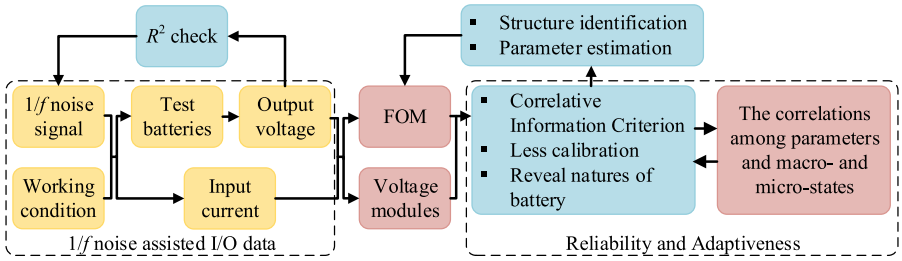

Fig. 1. Roadmap of this paper.

tery is acquired by applying sine wave with a magnitude of 10 mA and frequency ranging from 0.05 Hz to 10^2 kHz. 120 impedance points are recorded with uniform frequency interval. In the characteristic test, the input current and output voltage are synchronously recorded at a sampling frequency of 1 Hz, including the static capacity test, the open circuit voltage test and the charge and discharge tests. The infinite impulse response (IIR) filtering technology can be applied if the dynamic or online acquisition of EIS is required.

Dataset

EIS from electrochemical test

EIS describes the impedance characteristic along with the change of the frequency of sine current. It is usually used to analyze the polarization, electric double layer, diffusion of battery and other characteristics inside battery [26,35]. In this paper, the tested EIS is applied to determine the model structure and initially estimate model parameters. All EIS data from batteries with different SOH are collected and presented as shown in Fig. 3. SOH is defined as the ratio of maximum capacity to rated capacity. The maximum capacity is acquired by static capacity testing, which should be higher than 80% of the rated capacity[36]. 7 batteries with SOH greater than 80% are selected and numbered as *T-1006*, *T-1025*, *T-1109*, *T-1110(1)*, *T-1110(2)*, *T-1111(1)* and *T-1111(2)*. Their SOHs are shown in Table 1.

Input current from battery characteristic test

It is well known that most disturbances in the battery usage environments follow the characteristics of $1/f$ noise[37,38]. In order to stimulate more dynamic characteristics and protect the battery, a nondestructive $1/f$ noise signal is superimposed to the input current, where the $1/f$ noise is optimized by the R^2 index [39]. It is more appropriate when R^2 is closer to 1, and the detailed description of R^2 will be shown later. The maximum amplitude of the nondestructive $1/f$ noise signal is one-tenth of the amplitude of the maximum input current.

Output voltage from battery characteristic test

Based on the above additive $1/f$ noise assisted input, the discharge tests of the lithium iron phosphate batteries (LiShen, rated voltage 3.2 V and rated capacity 31 Ah) with different SOH are carried out, and the corresponding voltage signals are acquired. The voltage signals from the above superimposed input signal show as fluctuating curves. They enrich the dynamic characteristics of battery, and meet the requirements to find eigen-voltages.

Fractional-order modeling

Structure identification

Battery ECM can be acquired from the analysis of EIS that provides insights into the electrochemical systems and represents the internal dynamic processes of the battery. The corresponding relations between battery ECM and EIS are shown in Fig. 4. The dotted line that denotes EIS is divided into three regions according to different frequency domains and corresponding to different electrochemical reactions.

In the low-frequency region (right most red dotted oblique curve), typically below 1 Hz, EIS describes the diffusion process of electrochemical reactions, which is presented as the Warburg impedance.

In the middle-frequency region (with green dots on it), usually between 1 Hz and 1 kHz, EIS describes the electric double-layer effect of battery as well as the charge transfer process of lithium-ion and electron at the conductive junction, which is presented as part of the circle above $-Z_{im} = 0$. A resistance and a double-layer capacitance are generated in this process, which is presented as a RC pair.

The high-frequency region (left most red dotted curve), generally above 1 kHz, describes the movement of charge carried

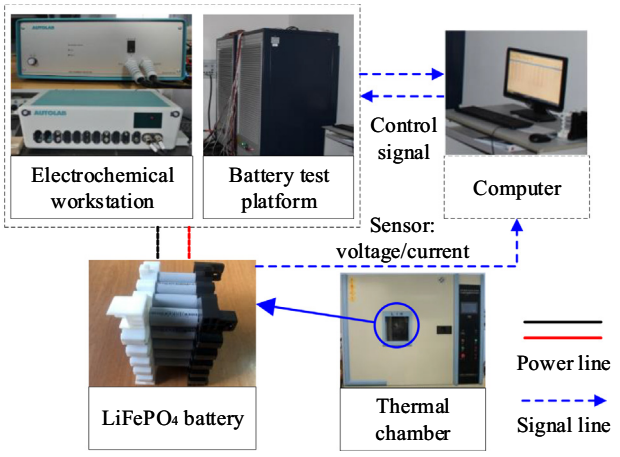

Fig. 2. Battery test scheme.

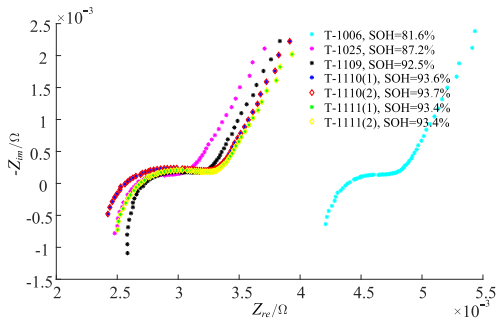

Fig. 3. EIS curves for batteries with different SOH.

Table 1
SOH of tested batteries.

Bettery No.	*T-1006*	*T-1025*	*T-1109*	*T-1110(1)*	*T-1110(2)*	*T-1111(1)*	*T-1111(2)*
SOH	81.6%	87.2%	92.5%	93.6%	93.7%	93.4%	93.4%

through the electrolyte and current collectors to the external circuit. In this region, the battery behavior is modeled by the ohmic resistance according to the intersection point R_0 between EIS and $-Z_{im} = 0$.

It follows that the fractional-order equivalent circuit model (FO-ECM) is composed by all equivalent circuit elements in the above-mentioned regions, i.e. the ohmic resistance, the RC pair and the Warburg impedance in series. The impedance of polarization capacitance is expressed as

$$Z_1(j\omega) = \frac{1}{C_1(j\omega)^{\alpha}}. \tag{1}$$

where C_1 is the fractional-order capacitance defined as a constant. The unit of C_1 is $\mathrm{F}\cdot\mathrm{sec}^{\alpha-1}$ to meet the dimensional requirements [25,26]. The physical meanings of C_1 in fractional-order elements point to the process of electric double-layer effect and transfer reaction at the electrode surfaces [19,28]. j is the imaginary number. ω is the radian frequency and α is the fractional-order of polarization capacitance. If $\alpha = 1$, the polarization capacitance is an ideal capacitor. Otherwise, if $0 < \alpha < 1$, the capacitance is a constant phase element (CPE). Moreover, the order of Warburg element is around 1/2 or 1/4 for lithium-ion batteries or fuel cells, respectively [40,41]. Actually, in battery characteristic test, the Warburg impedance is too small to be considered. Therefore, in this paper, the FO-ECM is composed of a resistance (R_0) in series with a RC pair ($R_1//C_1$) in Fig. 4.

Parameter estimation

Based on the above structure information, the impedance of FO-ECM (see Fig. 4 without considering the Warburg impedance) is expressed as

$$Z = R_0 + \frac{R_1}{1 + R_1C_1(j\omega)^{\alpha}}. \tag{2}$$

The real part Z_{Re} and imaginary part Z_{Im} of Z are acquired by Eulerian formulations, i.e.

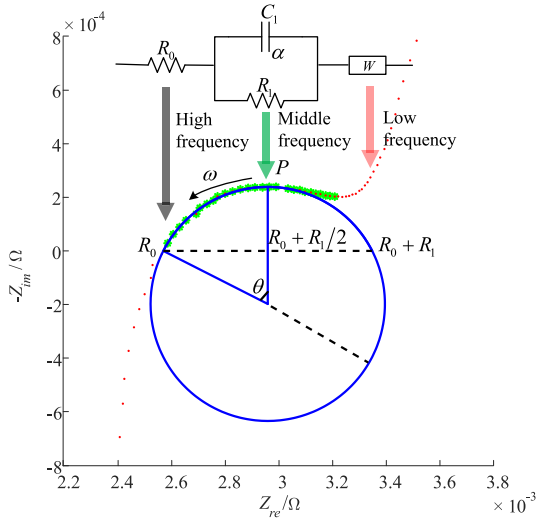

Fig. 4. Equivalent circuit analogous in impedance spectroscopy.

$$Z_{\mathrm{Re}} = R_0 + \frac{R_1\left(1 + R_1C_1\omega^{\alpha}\cos\frac{\alpha\pi}{2}\right)}{1 + 2R_1C_1\omega^{\alpha}\cos\frac{\alpha\pi}{2} + (R_1C_1\omega^{\alpha})^2}, \tag{3}$$

$$Z_{\mathrm{Im}} = -\frac{R_1^2C_1\omega^{\alpha}\sin\frac{\alpha\pi}{2}}{1 + 2R_1C_1\omega^{\alpha}\cos\frac{\alpha\pi}{2} + (R_1C_1\omega^{\alpha})^2}. \tag{4}$$

It follows from Eqs. (2)–(4) that Z can be expressed as

$$\left[Z_{\mathrm{Re}} - \left(R_0 + \frac{R_1}{2}\right)\right]^2 + \left(Z_{\mathrm{Im}} + \frac{R_1}{2}\cot\frac{\alpha\pi}{2}\right)^2 = \left(\frac{2}{R_1}\sin\frac{\alpha\pi}{2}\right)^{-2}, \tag{5}$$

where $(R_0 + R_1/2, -R_1\cot(\alpha\pi/2)/2)$ is the center of circle (5) as well as the center of the fitted curve (green dotted curve) in Fig. 4. It further follows from

$$R_1\cot(\alpha\pi/2)/2 = R_1\cot\theta/2, \tag{6}$$

that the fractional-order α is

$$\alpha = 2\theta/\pi. \tag{7}$$

Besides, in Fig. 4, the highest point P on the circle denotes that

$$R_0 + \frac{R_1\left(1 + R_1C_1\omega_p^{\alpha}\cos\frac{\alpha\pi}{2}\right)}{1 + 2R_1C_1\omega_p^{\alpha}\cos\frac{\alpha\pi}{2} + \left(R_1C_1\omega_p^{\alpha}\right)^2} = R_0 + \frac{R_1}{2}, \tag{8}$$

where ω_p^{α} is the frequency value at P. The polarization capacitance C_1 of the CPE is acquired by solving (8), i.e.

$$C_1 = 1/\left(R_1\omega_p^{\alpha}\right). \tag{9}$$

The calculations of parameters in FO-ECM are summarized in Table 2. Furthermore, the polarization effect leads to significant changes of EIS and fitting errors of FO-ECM in time domain. Existing literatures [34] and the observations of many EIS plots indicate that the accuracy of FO-ECM can be effectively improved by tuning polarization resistance R_1 and polarization capacitance C_1, which will also be verified in the correlation analysis later in this paper. To this end, a proportional learning law for R_1 and C_1 is designed to optimize FO-ECM, which is expressed as

$$\vartheta_{n+1} = \vartheta_n + \mathrm{sgn}(\cdot)\Gamma\|e_n\|_{\infty}, \tag{10}$$

where the estimated parameters in the n_{th} iteration denote as $\vartheta_n = (R_{1n}, C_{1n})^T$. $e_n = y - y_n, y$ and y_n are the tested and modeled voltage signal, respectively. Besides, n starts at 1 and ends at the cut-off condition, such as $\|e_n\|_{\infty} \leqslant \epsilon$, where $\epsilon > 0$ is the permitted error. The symbolic function $\mathrm{sgn}(\cdot)$ in (10) is defined as

$$\mathrm{sgn}(\cdot) = \begin{cases} 1, & |\max(e_n)| = \|e_n\|_{\infty} \\ -1, & |\min(e_n)| = \|e_n\|_{\infty} \end{cases}, \tag{11}$$

where $\|e_n\|_{\infty}$ denotes the infinite norm of error. $|\max(e_n)|$ and $|\min(e_n)|$ are the absolute values of the maximum and minimum errors, respectively. When $|\max(e_n)| = \|e_n\|_{\infty}$, the fitted voltage signal is considered to move up compared to the test voltage signal, and the symbolic function takes 1. When $|\min(e_n)| = \|e_n\|_{\infty}$, the fitted voltage signal is considered to move down compared to the test voltage signal, and the symbolic function takes -1. Besides, Γ is the positive learning gain that guarantees the convergence of (10), and can be tuned in one direction. The efficiency of the above ILI algorithm is illustrated in [42–44]. It should be noted that the learning law (10) also works for all parameters of FO-ECM, including α. A

Table 2
Parameter calculation formula for FO-ECM.

Parameter name	Calculation formula
R_0	The left intersection of ECM and $-Z_{im}=0$
R_1	The distance between two intersections of ECM and $-Z_{im}=0$
C_1	$1/\left(R_1\omega_p^{\alpha}\right)$
α	$2\theta/\pi$

proper selection of the parameters can reduce computational burden, and guarantee modeling precision.

Model evaluation

Accuracy evaluation

Taking the lithium iron phosphate battery No. *T-1110(1)* as an example, its model structure and initial model parameters are identified by the EIS analysis. Then, R_1 and C_1 are optimized by the iterative learning algorithm with learning gain $\Gamma=0.0012$. Thanks to the initial estimations in EIS, a small gain guarantees fast convergence of R_1 and C_1. The cut-off condition reaches at the 11_{th} iteration. Meanwhile, as comparison, the widely used genetic algorithm is applied to estimate the parameters in FO-ECM, which are shown in Table 3.

Let the tested voltage as reference, and based on the two groups of parameters in Table 3, the fitting results (errors) are shown in Fig. 5. For battery No. *T-1110(1)*, Fig. 5(a) and (b) are the output voltage fittings by using iterative learning algorithm and genetic algorithm, respectively. The corresponding input current is in the superposition of 1/3C constant current and an $1/f$ noise whose module of scalar is in one-tenth of the current amplitude. Fig. 5 (c) and (d) are the corresponding fitting errors. In order to distinguish their fitting effects, the root-mean square error (RMSE) and the maximum absolute error (MAE) are applied. The fitting results (Table 4) shows that the iterative learning algorithm performs better than the genetic algorithm one, which are held for both RMSE and MAE indices. As a result, the FO-ECM optimized by iterative learning algorithm and analyzed by EIS is feasible and accurate, which is the basis in the following correlative analysis.

Structure and parameter evaluations

An ideal model with precise structure and parameters should partially relevant to various internal and external states. To reveal this relevance, the correlation analysis among eigen-voltages and model parameters is carried out.

Scale-free network and eigen-voltages

Temporarily put model evaluation aside, and look back to the R^2 check for $1/f$ noise. Given a scale-free of network, whose distributions for frequency $p(k)$ and connectivity of nodes k follow the inverse power distribution $p(k)\sim k^{-\gamma}$, the R^2 index is defined as the square of correlation between $\log(p^k)$ and $\log(k)$. In particular, the connectivity k_i for the i_{th} node is defined as $k_i=\sum_{j=1}^{n}\omega_{ij}$, where ω_{ij} is the topological overlap between the node i and node j, and n is the number of nodes.

In order to build a scale-free network by using the $1/f^{\alpha}$ noise assisted voltage, where $1/f^{\alpha}$ denotes the response of $1/f$ noise for FO-ECM, the weighted co-expressed network analysis (WCNA) [39] is applied to generate scale-free networks. Besides, the output voltage can be further grouped and tagged in the module trait relation diagram by using average linkage hierarchical clustering method. The traits described in the module trait relation diagram are model parameters. For clarity, the voltage data at certain sampling instants are defined as the nodes of scale-free network. Besides the model parameters, any other battery micro- and macro-states with different dimensions can be defined as traits, which is beyond the scope of this paper.

Allow for different capacities and SOHs of the tested batteries, the selection of nodes is specified as follows. Firstly, intercept the output voltage data ranging from 20% SOC to 90% SOC of the battery with the shortest lifetime as benchmark sample. The nodes in the benchmark sample are corresponding to the SOC values of battery. Then, according to each SOC, the voltage signal ranging from 20% SOC to 90% SOC of another eight batteries are intercepted. Finally, according to each SOC, the samples of batteries with different SOHs are collected in a standard sample set V. In this paper, the data set V is a 7×1900 dimension matrix corresponding to 7 samples and 1900 nodes.

As for the traits, according to the iterative learning algorithm, the FO-ECM parameters of 7 batteries are collected in Table 5. Then, the trait set T_{FO-ECM} is acquired to build the module trait relation diagram, which is a 7×4 dimensional matrix corresponding to 4 traits (α,R_0,R_1,C_1) and 7 samples.

According to the standard sample set V and WCNA method, the scale-free network is acquired by the correlation and topological overlap calculation between any two nodes, and the module is generated by the average linkage hierarchical clustering method. Then, coupled with the trait set T_{FO-ECM}, the module trait relation diagram is acquired by the correlation between the eigen-voltage (hub node) in each module and each trait (Fig. 6(a)).

Correlative information criterion and comprehensive evaluations

Based on the analysis of the network modules and the idea of multiple correlation coefficient, a correlative information criterion (CIC) is proposed to evaluate the structure and parameters of various battery models, which consists of two parts, i.e. the establishment of regression model, and the calculation of multiple correlation coefficient.

The regression model between each model parameter and confidence eigen-voltages is described as (12).

$$\mathbf{y}=\mathbf{A}\hat{\mathbf{x}}+\epsilon \quad \text{and} \quad \hat{\mathbf{y}}=\mathbf{A}\hat{\mathbf{x}}, \tag{12}$$

where $\mathbf{y}$ is any model parameter vector in Table 5, ϵ is the error term, $\hat{\mathbf{x}}=[\hat{x}_1\ \ \hat{x}_2\ \ \cdots\ \ \hat{x}_m]^T$ is a coefficient vector in regression model, $\hat{\mathbf{y}}=[\hat{y}_1\ \ \hat{y}_2\ \ \cdots\ \ \hat{y}_n]^T$ is an regressive parameter vector, m is the number of confidence modules and n is the number of samples ($n=7$ in this paper). Besides,the column vector $\mathbf{a}_i=[a_{i1}\ \ a_{i2}\ \ \cdots\ \ a_{in}]^T$ in $\mathbf{A}=[\mathbf{a}_1\ \ \mathbf{a}_2\ \ \cdots\ \ \mathbf{a}_m]$ is the eigen-voltage of the i_{th} confidence module satisfying high Pearson correlation and p-value≤ 0.1 (Fig. 6), where $i\in\{1,2,\cdots,m\}$ and $m\leqslant n$, so that

Table 3
Estimated parameters in FO-ECM for battery No.*T-1110(1)*.

parameter name	R_0	R_1	C_1	α
Iterative learning algorithm	2.569e−03	7.272e−03	1.138e+02	7.004e−01
Genetic algorithm	2.892e−03	7.476e−03	6.156e+02	6.0292e−01

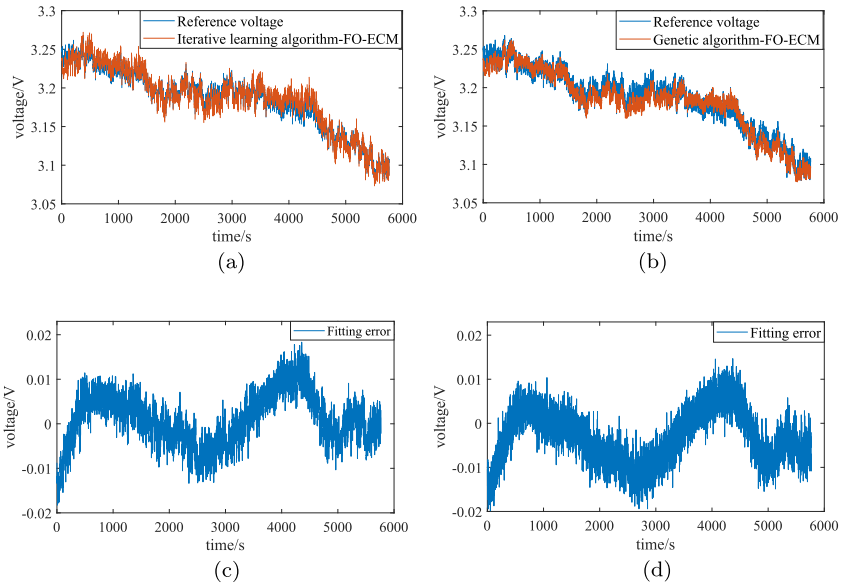

Fig. 5. Output voltage fittings for FO-ECM based on different estimation algorithms: (a) voltage fitting based on iterative learning algorithm at 20–90% SOC; (b) voltage fitting based on genetic algorithm at 20–90% SOC; (c) fitting error for iterative learning algorithm; (d) fitting error for genetic algorithm.

Table 4
Fitting accuracies for FO-ECM with different parametric estimation algorithms.

	Iterative learning algorithm	Genetic algorithm
RMSE	0.0059	0.0061
MAE	0.0183	0.0199

$A_{n\times m}$ is column full rank. The selected eigen-voltages corresponding each parameter and their Pearson correlations are listed in Fig. 6(b).

The multiple correlation coefficient between model parameter vector **y** and eigen-voltage vectors $\mathbf{a}_i$ in **A** is named as "Correlative Information Criterion (CIC)" of **y**, and calculated by (13).

$$\mathrm{CIC}_{\mathbf{y}} = \frac{\sqrt{\sum_{k=1}^{n}(y_k-\bar{y})^2}}{\sqrt{\sum_{k=1}^{n}(\hat{y}_k-\bar{y})^2}}, \tag{13}$$

where $\bar{y} = \sum_{k=1}^{n} y_k/n$.

The CIC as well as some other indices for FO-ECM (Table 5) are shown in Table 6. The residual standard error is used to measure the fitting degree of (12) and the smaller the better. Significant F is the F_α critical value at the significance level. If the F-statistic is greater than the critical value, the null hypothesis is refused and the regression model has a good regression effect. Coupled with the module trait relations in Fig. 6, CIC and correlativity describe the correlation coefficient and relation between any model parameter and its confidence eigen-voltages, respectively.

Then, after comprehensively analyzing the CIC indices (Table 6) and the correlations between model parameters and SOH, let's focus on the parameters of FO-ECM one may interested. For the ohmic resistance R_0, it can be seen in Table 6 that CIC_{R_0} is 0.9348 and its correlation with SOH (Table 1) is $r_{R_0} = -0.873$, which indicates that R_0 is sensitive to the eigen-voltages (working conditions)

Table 5
Parameters of FO-ECM.

Battery No.	*T-1006*	*T-1025*	*T-1109*	*T-1110(1)*	*T-1110(2)*	*T-1111(1)*	*T-1111(2)*
α	6.504e−01	6.357e−01	7.123e−01	7.004e−01	7.004e−01	6.745e−01	6.745e−01
R_0	4.397e−03	2.654e−03	2.728e−03	2.569e−03	2.569e−03	2.689e−03	2.689e−03
R_1	7.944e−03	6.064e−03	7.603e−03	7.300e−03	8.019e−03	7.302e−03	7.940e−03
C_1	1.274e+02	2.871e+02	1.819e+02	1.138e+02	1.138e+02	1.503e+02	1.503e+02

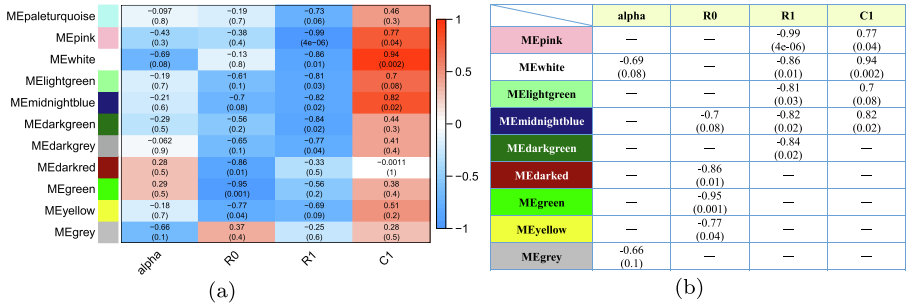

	alpha	R0	R1	C1
MEpink	—	—	-0.99 (4e-06)	0.77 (0.04)
MEwhite	-0.69 (0.08)	—	-0.86 (0.01)	0.94 (0.002)
MElightgreen	—	—	-0.81 (0.03)	0.7 (0.08)
MEmidnightblue	—	-0.7 (0.08)	-0.82 (0.02)	0.82 (0.02)
MEdarkgreen	—	—	-0.84 (0.02)	—
MEdarked	—	-0.86 (0.01)	—	—
MEgreen	—	-0.95 (0.001)	—	—
MEyellow	—	-0.77 (0.04)	—	—
MEgrey	-0.66 (0.1)	—	—	—

Fig. 6. (a) Module trait relations of FO-ECM. Here the voltage modules and model parameters are positioned on vertical and horizontal axis, respectively. These voltage modules are obtained from the output voltage matrix. The Pearson correlation between each eigen-voltage and model parameter as well as its significance level are calculated. The meter of correlation is shown on the right; (b) Pearson correlation and significance level (p-value) from (a), where p-value is in parentheses.

Table 6
Correlative information criterion of model parameters.

	Residual standard error	CIC	Correlativity	F-statistic	Significant F
α	2.087e−02	0.6335	Negative	3.457	0.1343
R_0	2.933e−04	0.9348	Negative	7.17	0.1261
R_1	1.547e−04	0.9919	Negative	24.53	0.1521
C_1	19.6	0.9653	Positive	13.9	0.06822

and SOH. Similarly, analyzing CIC_{R_1} and CIC_{C_1} as well as those correlations $r_{R_1} = 0.098$ and $r_{C_1} = -0.256, R_1$ and C_1 are sensitive to the eigen-voltages (working conditions), but almost invariant with the change of SOH. For the fractional-order $\alpha, \mathrm{CIC}_\alpha = 0.6335$ and $r_\alpha = 0.73$ are relatively low, which imply that α in FO-ECM can be set as constant for different working conditions and SOHs. In particulary, R_0 is the parameter with the strongest correlation to SOH, which can be regarded as the vane of SOH. As a by-product, the existence of confidence CICs indicates that the structure of the above FO-ECM is reliable and adaptive. Therefore, the structure identification, the parameter estimation and the ability of revealing natures of battery have be achieved in this paper.

Conclusions

In this paper, a FO-ECM is established by determining the structure identification and initial estimation of parameters with EIS, and by tuning the polarization affected parameters with iterative learning algorithm. Meanwhile, a $1/f$ noise is introduced and optimized subject to R^2 index, which is an essential to reveal reliable correlations between model parameters and eigen-voltages. As a result, the multiple correlation between any parameter and confidence eigen-voltages is defined as CIC index. The CIC indices are available to evaluate the structure and parameters of various battery models, as well as expected to find reliable relations between model parameters and micro- or macro-states.

Moreover, the main observation and the main conclusion of our study, which can be of importance and usefulness for practical applications of lithium-ion batteries, is that, in the modeling approach used in this paper, the fractional-order α can be assumed as a constant (namely, constant $\alpha \in [0.6357, 0.7123]$ in our study). We hope to find explanation to this fact using the porous functions approach [45] for describing the structure of the battery material and processes in it.

Compliance with Ethics Requirements

This article does not contain any studies with human or animal subjects.

Declaration of Competing Interest

The authors declare that they have no known competing financial interests or personal relationships that could have appeared to influence the work reported in this paper.

References

[1] Dai H, Jiang B, Wei X. Impedance characterization and modeling of lithium-ion batteries considering the internal temperature gradient. Energies 11 (1). doi:10.3390/en11010220.

[2] Ajadi T, Boyle R, Strahan D, Kimmel M, Collins B, Cheung A, et al. Global trends in renewable energy investment 2019; 2019. doi:http://hdl.handle.net/20.500.11822/29752.

[3] Song Y, Xia Y, Lu Z. Integration of plug-in hybrid and electric vehicles: Experience from China; 2010. doi:10.1109/PES.2010.5589926.

[4] Krishnan HS, Senthil KV. A nonlinear equivalent circuit model for lithium ion cells. J Power Sources 2013;222:210–7. doi: https://doi.org/10.1016/j.jpowsour.2012.08.090.

[5] Hannan M, Lipu M, Hussain A, Mohamed A. A review of lithium-ion battery state of charge estimation and management system in electric vehicle applications: Challenges and recommendations. Renew Sustain Energy Rev 2017;78:834–54. doi: https://doi.org/10.1016/j.rser.2017.05.001.

[6] Wei Z, Zou C, Leng F, Soong BH, Tseng K-J. Online model identification and state-of-charge estimate for lithium-ion battery with a recursive total least squares-based observer. IEEE Trans Industr Electron 2017;65(2):1336–46. doi: https://doi.org/10.1109/TIE.2017.2736480.

[7] Wei Z, Leng F, He Z, Zhang W, Li K. Online state of charge and state of health estimation for a lithium-ion battery based on a data-model fusion method. Energies 11 (7). doi:10.3390/en11071810.

[8] Wei J, Dong G, Chen Z. On-board adaptive model for state of charge estimation of lithium-ion batteries based on Kalman filter with proportional integral-based error adjustment. J Power Sources 2017;365:308–19. doi: https://doi.org/10.1016/j.jpowsour.2017.08.101.

[9] Doyle M, Fuller T, Newman J. Modeling of galvanostatic charge and discharge of the lithium/polymer/insertion cell. J Electrochem Soc 1993;140(6):1526–33. doi: https://doi.org/10.1149/1.2221597.

[10] Rahman MA, Anwar S, Izadian A. Electrochemical model parameter identification of a lithium-ion battery using particle swarm optimization method. J Power Sources 2016;307:86–97. doi: https://doi.org/10.1016/j.jpowsour.2015.12.083.

[11] Li J, Wang L, Lyu C, Liu E, Xing Y, Pecht M. A parameter estimation method for a simplified electrochemical model for Li-ion batteries. Electrochim Acta 2018;275:50–8. doi: https://doi.org/10.1016/j.electacta.2018.04.098.

[12] Gong X, Rui X, Mi CC. A data-driven bias-correction-method-based lithium-ion battery modeling approach for electric vehicle applications. IEEE Trans Ind Appl 2016;52(2):1759–65. doi: https://doi.org/10.1109/TIA.2015.2491889.

[13] Pang H, Zhang F. Experimental data-driven parameter identification and state of charge estimation for a Li-ion battery equivalent circuit model. Energies 11 (5). doi:10.3390/en11051033.

[14] Zhang X, Lu J, Yuan S, Yang J, Zhou X. A novel method for identification of lithium-ion battery equivalent circuit model parameters considering electrochemical properties. J Power Sources 2017;345:21–9. doi: https://doi.org/10.1016/j.jpowsour.2017.01.126.

[15] Mu H, Xiong R, Zheng H, Chang Y, Chen Z. A novel fractional order model based state-of-charge estimation method for lithium-ion battery. Appl Energy 2017;207:384–93. doi: https://doi.org/10.1016/j.apenergy.2017.07.003.

[16] Tian J, Xiong R, Yu Q. Fractional-order model-based incremental capacity analysis for degradation state recognition of lithium-ion batteries. IEEE Trans Industr Electron 2019;66(2):1576–84. doi: https://doi.org/10.1109/TIE.2018.2798606.

[17] Shang Y, Qi Z, Cui N, Zhang C. Research on variable-order RC equivalent circuit model for lithium-ion battery based on the AIC criterion. Trans China Electrotech Soc 2015;30(17):55–62. CNKI:SUN:DGJS.0.2015-17-006.

[18] Berrueta A, Urtasun A, Ursúa A, Sanchis P. A comprehensive model for lithium-ion batteries: From the physical principles to an electrical model. Energy 2018;144:286–300. doi: https://doi.org/10.1016/j.energy.2017.11.154.

[19] Wang B, Li SE, Peng H, Liu Z. Fractional-order modeling and parameter identification for lithium-ion batteries. J Power Sources 2015;293:151–61. doi: https://doi.org/10.1016/j.jpowsour.2015.05.059.

[20] Xia F, Yuan B, Peng D, Zhang H. Modeling and optimization of variable-order RC equivalent circuit model for lithium ion batteries based on information criterion. Proc Chinese Soc Electrical Eng 2018; 38 (21): 6441–6451. doi:10.13334/j.0258-8013.pcsee.171235.

[21] Hu X, Li S, Peng H. A comparative study of equivalent circuit models for Li-ion batteries. J Power Sources 2012;198:359–67. doi: https://doi.org/10.1016/j.jpowsour.2011.10.013.

[22] Grandjean T, McGordon A, Jennings P. Structural identifiability of equivalent circuit models for Li-ion batteries. Energies 10 (1). doi:10.3390/en10010090.

[23] Akaike H. A new look at the statistical model identification. IEEE Trans Autom Control 1974;19(6):716–23. doi: https://doi.org/10.1109/TAC.1974.1100705.

[24] Qi M, Zhang GP. An investigation of model selection criteria for neural network time series forecasting. Eur J Oper Res 2001;132(3):666–80. doi: https://doi.org/10.1016/S0377-2217(00)00171-5.

[25] Westerlund S, Ekstam L. Capacitor theory. IEEE Trans Dielectr Electr Insul 1994;1(5):826–39. doi: https://doi.org/10.1109/94.326654.

[26] Zou C, Zhang L, Hu X, Wang Z, Wik T, Pecht M. A review of fractional-order techniques applied to lithium-ion batteries, lead-acid batteries, and

supercapacitors. J Power Sources 2018;390:286–96. doi: https://doi.org/10.1016/j.jpowsour.2018.04.033.
[27] V. Martynyuk, M. Ortigueira, Fractional model of an electrochemical capacitor, Signal Processing 107 (feb.) (2015) 355–360. doi:10.1016/j.sigpro.2014.02.021.
[28] Barsoukov E, Macdonald RJ. Impedance spectroscopy: theory, experiment, and applications. Wiley-Interscience; 2005. doi:10.1002/0471716243.
[29] Lopes AM, Machado JAT, Ramalho E, Silva V. Milk characterization using electrical impedance spectroscopy and fractional models. Food Anal Meth 2018;11:901–12. doi: https://doi.org/10.1007/s12161-017-1054-4.
[30] Samadani E, Farhad S, Scott W, Mastali M, Gimenez LE, Fowler M, et al. Empirical modeling of lithium-ion batteries based on electrochemical impedance spectroscopy tests. Electrochim Acta 2015;160:169–77. doi: https://doi.org/10.1016/j.electacta.2015.02.021.
[31] Yu Z, Xiao L, Li H, Zhu X, Huai R. Model parameter identification for lithium batteries using the coevolutionary particle swarm optimization method. IEEE Trans Industr Electron 2017;64(7):5690–700. doi: https://doi.org/10.1109/TIE.2017.2677319.
[32] Ranjbar AH, Banaei A, Khoobroo A, Fahimi B. Online estimation of state of charge in li-ion batteries using impulse response concept. IEEE Trans Smart Grid 2012;3(1):360–7. doi: https://doi.org/10.1109/TSG.2011.2169818.
[33] Alavi S, Birkl C, Howey D. Time-domain fitting of battery electrochemical impedance models. J Power Sources 2015;288:345–52. doi: https://doi.org/10.1016/j.jpowsour.2015.04.099.
[34] Waag W, Käbitz S, Sauer DU. Experimental investigation of the lithium-ion battery impedance characteristic at various conditions and aging states and its influence on the application. Appl Energy 2013;102:885–97. doi: https://doi.org/10.1016/j.apenergy.2012.09.030.
[35] Hu X, Hao Y, Zou C, Li Z, Zhang L. Co-estimation of state of charge and state of health for lithium-ion batteries based on fractional-order calculus. IEEE Trans Veh Technol 2018;67(11):10319–29. doi: https://doi.org/10.1109/TVT.2018.2865664.
[36] Shen P, Ouyang M, Lu L, Li J, Feng X. The co-estimation of state of charge, state of health, and state of function for lithium-ion batteries in electric vehicles. IEEE Trans Veh Technol 2018;67(1):92–103. doi: https://doi.org/10.1109/TVT.2017.2751613.
[37] Ye B, Li H-J, Ma X-P. $1/f^{\alpha}$ noise in spectral fluctuations of complex networks. Physica A 2010;389(22):5328–31. doi: https://doi.org/10.1016/j.physa.2010.07.023.
[38] Erland S, Greenwood PE, Ward LM. "$1/f^{\alpha}$ noise" is equivalent to an eigenstructure power relation. Europhys Lett 95 (6). doi:10.1209/0295-5075/95/60006.
[39] Zhang B, Horvath S. A general framework for weighted gene co-expression network analysis. Stat Appl Genetics Mol Biol 2005;4(1):i–43. doi: https://doi.org/10.2202/1544-6115.1128.
[40] Xu J, Mi CC, Cao B, Cao J. A new method to estimate the state of charge of lithium-ion batteries based on the battery impedance model. J Power Sources 2013;233:277–84. doi: https://doi.org/10.1016/j.jpowsour.2013.01.094.
[41] Andre D, Meiler M, Steiner K, Walz H, Soczka-Guth T, Sauer D. Characterization of high-power lithium-ion batteries by electrochemical impedance spectroscopy. ii: Modelling. J Power Sources 196(12), 2011,:5349–56. doi: https://doi.org/10.1016/j.jpowsour.2010.07.071.
[42] Abidi K, Xu J-X. Iterative learning control for sampled-data systems: From theory to practice. IEEE Trans Industr Electron 2011;58(7):3002–15. doi: https://doi.org/10.1109/TIE.2010.2070774.
[43] Zhao Y, Li Y, Zhou F, Zhou Z, Chen Y. An iterative learning approach to identify fractional order KiBaM model. IEEE/CAA J Autom Sin 2017;4(2):322–31. doi: https://doi.org/10.1109/JAS.2017.7510358.
[44] Bu X, Hou Z. Adaptive iterative learning control for linear systems with binary-valued observations. IEEE Trans Neural Netw Learn Syst 2018;29(1):232–7. doi: https://doi.org/10.1109/TNNLS.2016.2616885.
[45] Podlubny I. Porous functions. Fract Calculus Appl Anal 2019;22(6):1502–16. doi: https://doi.org/10.1515/fca-2019-0078.